nature communications

Article

https://doi.org/10.1038/s41467-024-54197-y

Feedback driven autonomous cycles of assembly and disassembly from minimal building blocks

Received: 8 July 2024

Accepted: 29 October 2024

Published online: 18 November 2024

Check for updates

Antara Reja[1,5], Sangam Jha[1,5], Ashley Sreejan[2,3], Sumit Pal[1], Subhajit Bal[1], Chetan Gadgil[2,3,4] & Dibyendu Das[1]

The construction of complex systems by simple chemicals that can display emergent network dynamics might contribute to our understanding of complex behavior from simple organic reactions. Here we design single amino acid/dipeptide-based systems that exhibit multiple periodic changes of (dis) assembly under non-equilibrium conditions in closed system, importantly in the absence of evolved biocatalysts. The two-component based building block exploits pH driven non-covalent assembly and time-delayed accelerated catalysis from self-assembled state to install orthogonal feedback loops with a single batch of reactants. Mathematical modelling of the reaction network establishes that the oscillations are transient for this network structure and helps to predict the relative contribution of the feedback loop to the ability of the system to exhibit such transient oscillation. Such autonomous systems with purely synthetic molecules are the starting point that can enable the design of active materials with emergent properties.

Living chemical reaction networks capable of progressive phase transitions played vital roles in the chemical emergence of life and driving the processes of extant biochemistry[1–15]. Living systems use both non-covalent assembly and covalent linkages to achieve complex behaviors such as oscillations. These catalytic reaction networks operate under non-equilibrium conditions that help to maintain the periodic changes of the constituents depending on the energy inputs[16–22]. Such periodic changes might have helped the systems to evolve towards higher complexity seen in contemporary metabolic networks[23–28]. Inspired by such complex natural systems, attempts have been made to synthetically realize systems that can exhibit periodic changes of one or more of its components or features such as pattern formation, aggregation behavior, and others[29–37]. To install this capability, the synthetic system is required to be integrated with the feedback loop as seen in the case of modern biochemical processes, from cell division to circadian rhythm[38–40]. Such, periodic changes in concentration of one or more components or oscillation have been demonstrated either by (1) employing inorganic molecules connected in a feedback loop (2) exploiting evolved enzymes or DNA, or (3) utilizing small organic molecules in the absence of non-covalent interactions in an open system[41–47]. Whereas, one of the fascinating examples of non-equilibrium chemical oscillator is Belousov-Zhabotinsky (BZ) reaction, where transition-metal ions catalyze the oxidation of organic reductants by bromic acid, resulting in colorful, oscillating patterns in a closed system[48]. We were interested in developing a system, completely comprising synthetic chemicals, that is capable of showing autonomous (dis)assembly cycles with periodic variation of concentration in a closed system utilizing non-covalent assembly and catalytic feedback loop. The non-triviality arises from the difficulty in incorporating delayed feedback in the absence of advanced biocatalysts in a closed system. Also, the dynamics of self-assembly of synthetic chemicals is generally limited by the relaxation towards chemical equilibrium[49–52]. Needless to say, if autonomous systems can be realized by utilizing purely synthetic molecules, then acutely

[1]Department of Chemical Sciences and Centre for Advanced Functional Materials, Indian Institute of Science Education and Research (IISER) Kolkata, Mohanpur 741246, India. [2]Chemical Engineering and Process Development, CSIR-National Chemical Laboratory, Pune 411008, India. [3]Academy of Scientific and Innovative Research (AcSIR), Ghaziabad 201002, India. [4]CSIR-Institute of Genomics and Integrative Biology, New Delhi 110025, India. [5]These authors contributed equally: Antara Reja, Sangam Jha. e-mail: dasd@iiserkol.ac.in

dynamic materials can be accessed with spatiotemporal control of properties.

Here, we report a simple design featuring a single amino acid/dipeptide that can self-assemble and disassemble autonomously in a closed system. The building block exploits non-covalent assembly, accelerated catalysis from self-assembled state and time-delayed formation of a dynamic covalent bond, to introduce feedback loop in a closed system with a single batch of reactants. Further, through mathematical modeling we have tried to illustrate the theoretical possibility that the described set of reactions and regulatory interactions can result in autonomous (dis)assembly cycles.

Results

Towards our goal to access a minimal chemical-based system capable of demonstrating multiple cycles of (dis)assembly, a two-component system was designed, which included negative and positive feedback with suitable time delay in kinetics under non-equilibrium conditions. Firstly, if the assembly is catalytic and can promote its own degradation, then the negative feedback could be installed (Fig. 1a). Further, if one of the products of the catalytic degradation or building block can facilitate the regeneration of the assembly, a time-delayed positive feedback will be installed (Fig. 1b). This coupling of negative and positive feedback loops might yield autonomous (dis)assembly for multiple cycles in a closed system (Fig. 1c). With these in mind, the building block **A'BC** was rationally designed (Fig. 1d). The building block features a kinetically stable but thermodynamically activated hydrophobic ester (**BC**, Fig. 1d). This aromatic ester has a free aldehyde group that can couple via a dynamic imine bond with the amine group present in the polar residue (**A'**) to access the amphiphilic building block **A'BC** which may have the propensity to self-assemble and promote its own formation in an aqueous medium (Fig. 1d). For the polar residue **A'**, molecular histidine was used (Fig. 1d). Free histidine usually has poor hydrolytic role yet they show an enhancement of their catalytic proficiencies when they are featured in supramolecular assemblies via multivalency, co-operative effects and so forth[4,53]. Finally, the dynamic imine bond was selected as this linkage is known for its acute responsiveness towards pH switches which was used to generate the second feedback (positive feedback). Hence, an ester was synthesized via the condensation of 4-formylbenzoic acid (**B**), and 4-nitrophenol (**C**), which was used as the hydrophobic part and, upon catalytic hydrolysis would create a pH gradient to provide positive feedback towards the imine bond formation (Fig. 1d).

Temporal gelation at pH 7.5 buffer (one cycle)

We started with a simplified system where only one feedback (hydrolytic activity) would be operational while the other would be inoperative (Fig. 2a). Hence, the feedback that could be generated from pH changes was deactivated by using a buffer system. **BC** was mixed with **A'** at different molar concentrations with a fixed molar ratio of 1:1 (DMSO/buffer solution, 60% v/v, pH 7.5). The samples with molar concentrations of 50 mM each (**A'** and **BC**) gradually became viscous, followed by the transformation into self-supporting gel at around 2 h (Fig. 2b). The gel showed weakening with time and manifested a gel-to-sol transition at 5 h (Fig. 2b). In the control experiments, **A'** was mixed with **B** under identical conditions and no gelation was observed within the similar timeframe (Supplementary Fig. 1).

The transient gels were monitored by visible light scattering spectroscopy ($\lambda = 700$ nm) to measure the turbidity of the system. The rapid increase in turbidity was observed till 2.5 h, which matched with the gelation time, followed by the gradual decrease that finally plateaued around ca. 11 h (Fig. 2e). To gain more insight into the temporal generation of the assembled state, transmission electron microscopy (TEM) was performed at different time intervals. TEM micrographs demonstrated that the temporal generation of self-assembled fibrillar

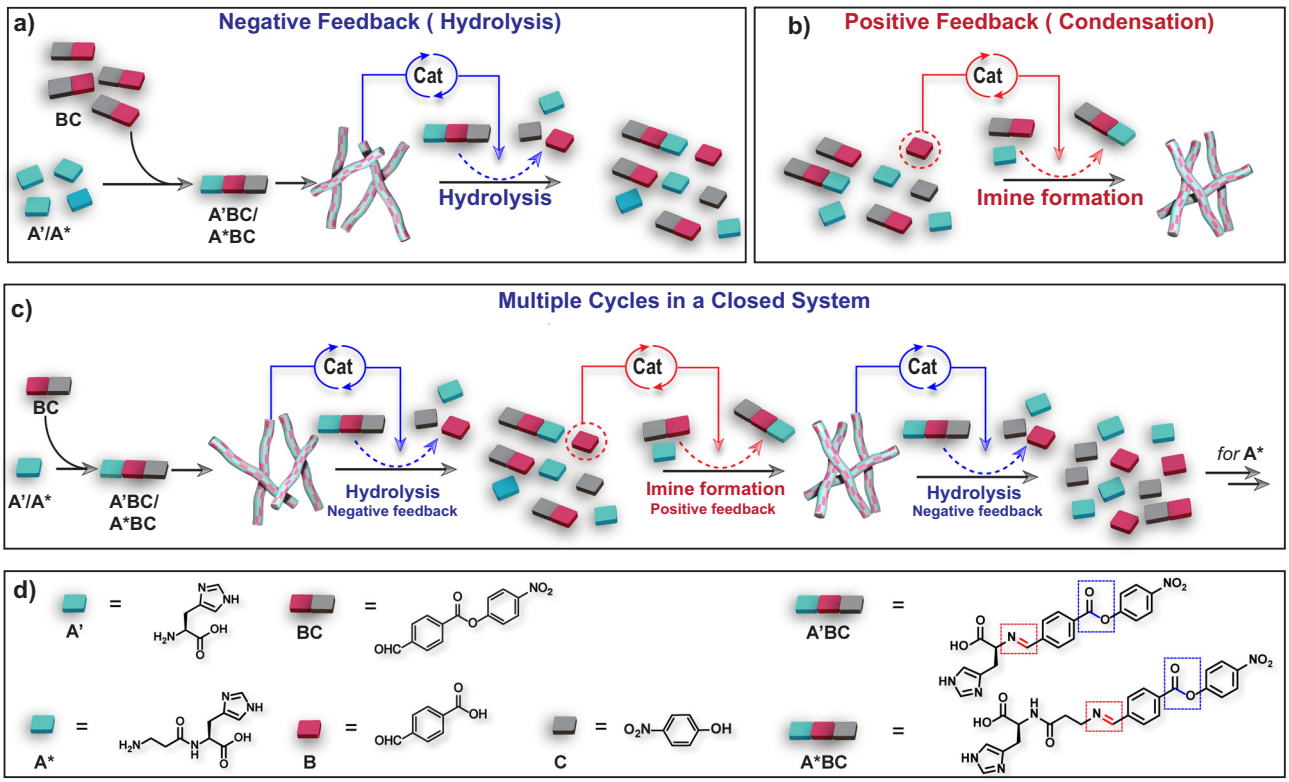

Fig. 1 | Schematic representation of dynamic self-assembly. Scheme showing **a** the generation of assembly and subsequent disassembly due to catalysis (negative feedback), **b** catalytic regeneration of assembly from the product (positive feedback) of the disassembly. **c** Integration of negative and positive feedback. **d** Symbols and their corresponding chemical structures.

https://doi.org/10.1038/s41467-024-54197-y

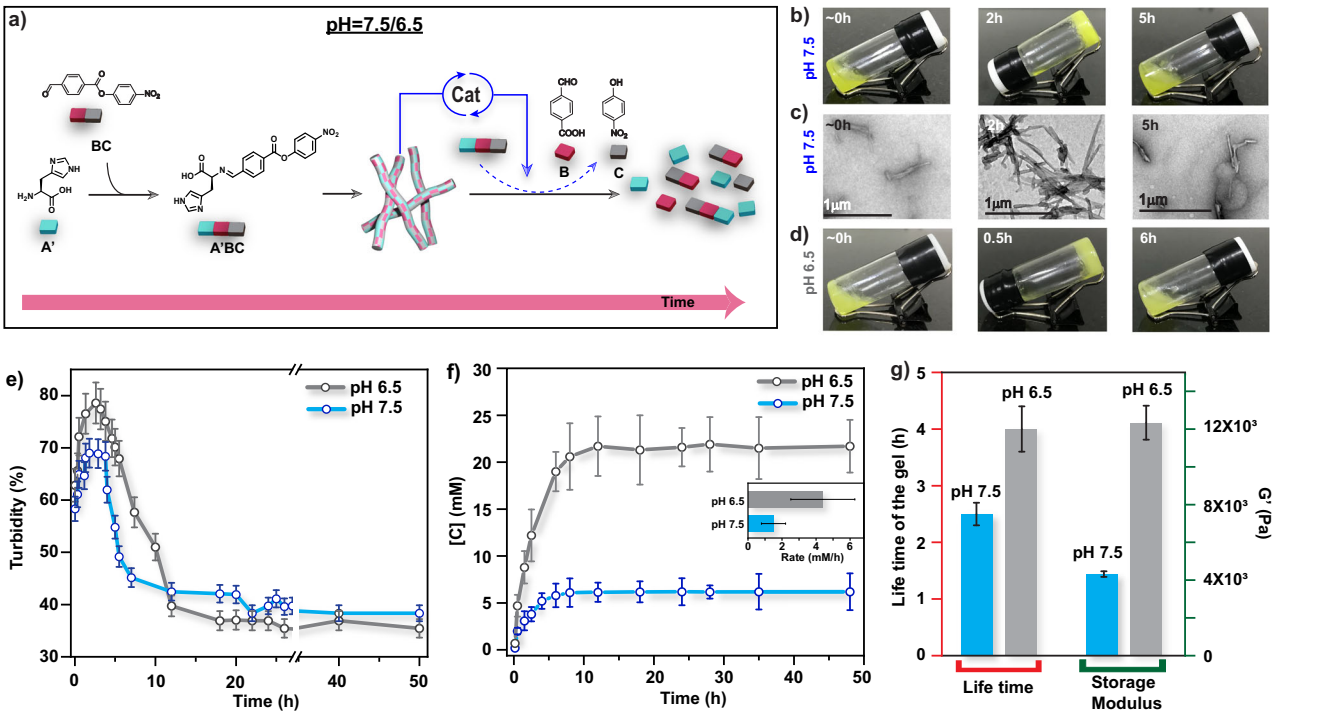

Fig. 2 | Gel formation and its catalytic activity at pH 7.5 and 6.5. a Schematic representation of the temporal generation of self-assembled structure at pH 7.5 and 6.5. Representative vial images at pH **b** 7.5 and **d** 6.5. **c** Time-dependent TEM images of pH 7.5 system. **e** Temporal change in turbidity at pH 7.5 and 6.5. **f** HPLC data of time-dependent concentration change of generated **C** in pH 7.5 and 6.5 systems. Inset shows the rate of **C** generation at pH 7.5 and 6.5 systems. **g** Lifetime (red) and storage modulus (green) of the gel state at pH 7.5 and 6.5. Error bars represent standard deviations of triplicate experiments.

structures was responsible for gelation. At time ~0 h, when the sample was in a sol state, sparsely populated fibrillar structures could be seen (Fig. 2c). However, at ca. 2 h (gel state), the network-like morphology was seen (Fig. 2c). After ca. 5 h, when the sample turned to sol, very few fibrillar structures could be seen (Fig. 2c). Further, the similar morphological transition was witnessed in scanning electron microscopy (SEM, Supplementary Fig. 2). Time-dependent rheology was performed to investigate the system in more detail on the macroscopic level. The gradual increase followed by the decrease (after 2 h) in storage modulus, confirmed the temporal change in material property of the system (Supplementary Figs. 3 and 4).

At this point, to investigate the self-assembly and autonomous disassembly process, both the imine and ester bonds were monitored by different analytical techniques. To probe the formation of imine bond, time-dependent nuclear magnetic resonance (NMR) spectroscopy was performed. ^{1}H NMR of the sample containing **A'** and **BC** (see methods section for more details) manifested the generation of imine with the proton peak at δ 8.41 ppm, which intensified till ca. 2 h. The formation of imine was also confirmed from HRMS analysis (Supplementary Fig. 5). The imine condensation, even with high proportion of water, suggested the role of the self-assembly process, as observed in previous reports[54]. Notably, the intensity of the peak started to decline after 2–3 h, which suggested the hydrolysis of the imine bond (Supplementary Fig. 6). The time gap in the increase and decrease of the imine peak intensity broadly corroborated with the lifetime of the gel. It is important to note here, the mixture of **A'** and **B** were free flowing and did not show any signs of gelation. NMR and HRMS of the mixture containing of **A'** and **B** also could not detect any imine formation. Further, the control molecule **DC** which lacked an aldehyde group, did not lead to self-assembly upon mixing with **A'** (Supplementary Fig. 7). These results underpinned that the self-assembling capabilities of the building block **A'BC** promoted the formation of the imine via self-templating. However, the quantification of the extent of imine formation was not possible due to NMR peak broadening, which resulted from the low mobility of the molecules at the assembled state. Further, considering the formation of imine product **A'BC** was driven by a self-assembly process, it was challenging to synthesize it in other solvents where it did not self-assemble.

To probe the coupling of the self-assembly process with catalysis, the hydrolysis of the ester (**BC**) was monitored via time-resolved high-performance liquid chromatography (HPLC). The rate of formation of **C** was monitored at $\lambda = 318$ nm (Fig. 2f). Notably, the rate profile showed an initial burst hydrolysis of the ester in the first 2.5 h with a hydrolytic rate of 1.5 mM/h. This rise was followed by a gradual decline of the rate and plateaued after 5 h. The initial burst suggested the assembled state was catalytic, while the sol state was unable to hydrolyze the remaining ester regardless of the presence of a large amount of histidine. This suggested that the self-assembly process was coupled with the catalytic hydrolysis and subsequently was responsible for its degradation, thus resulting in negative feedback. Control experiments done with a mixture of **C** with **A'** and **B** did not show the generation of any imine proton peak from NMR.

Temporal gelation at pH 6.5 buffer (one cycle)

As noted, the above experiments were done at pH 7.5. We were interested in investigating the system at a pH where the imine formation would be more favorable in the medium. For this, the pH of the medium was chosen to be 6.5 (DMSO/buffer, 0.1 M, 60% v/v) as low pH facilitates Schiff base formation via catalytic elimination of water[55]. At this pH, a mixture of **A'** and **BC** accessed a self-supporting gel within 0.5 h, which was significantly faster than the gelation time required at pH 7.5 (Fig. 2d, e). In contrast, when **A'** was mixed with **B** under identical conditions, no gelation was observed even at this low pH of the system (Supplementary Fig. 8). The gel at pH 6.5 was stable for a longer time (lifetime of 4 h compared to 2.5 h in case of pH 7.5, Fig. 2g). Further, the rapid rise in the turbidity in case of pH 6.5

https://doi.org/10.1038/s41467-024-54197-y

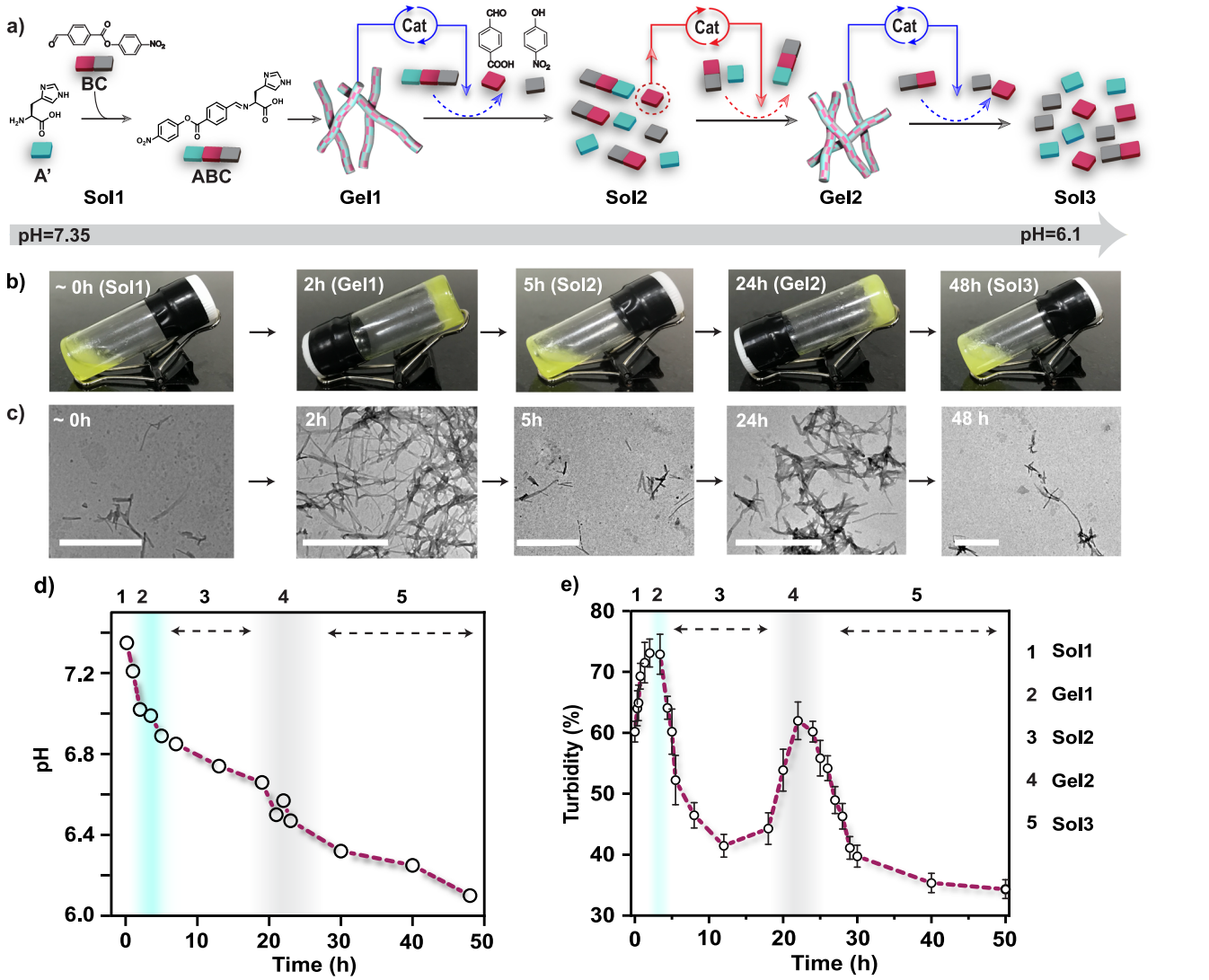

Fig. 3 | Autonomous pH change allows the regeneration of assembly. **a** Schematic representation of two autonomous cycles of (dis)assembly in the unbuffered medium in a closed system. **b** Representative vial images showing the temporal transition of different phases in an unbuffered system (done in 10 different sets of vials under identical experimental conditions). After 48 h, 6 out of 10 vials became viscous sol while the rest remained as a weak gel. **c** Time-dependent TEM images. All scale bars correspond to 1 μm. **d** Temporal change of pH in unbuffered medium. **e** Time-dependent change of turbidity in the unbuffered system. Error bars represent standard deviations of triplicate experiments.

compared to that observed for pH 7.5 supported the faster assembly in acidic pH (Fig. 2e). The prolonged lifetime was also confirmed from the turbidity measurement at pH 6.5. These observations suggested the rapid imine formation at acidic pH (6.5) facilitated a greater extent of building block (**A'BC**) generation that, in turn, led to longer lifetime of the self-assembled state. The greater extent of self-assembled networks was also supported by rheology measurements which showed improved mechanical strength of the gel (Fig. 2g, Supplementary Figs. 9 and 10).

The rate of hydrolysis at pH 6.5 was monitored by HPLC. The formation of **C** was seen to be accelerated significantly as it showed a burst release (for the first 0-3 h, 4.4 mM/h, Fig. 2f). Subsequently, the rate showed a decline (for 3–5 h, 1.7 mM/h) before plateauing after 5 h. The burst phase once again overlapped with the lifetime of the gel and reinforced the importance of the self-assembled catalytic microenvironment[49]. The rate of hydrolysis at pH 6.5 was almost three-fold higher than that was observed at pH 7.5 (Fig. 2f, inset). Higher hydrolytic rates at lower pH again supported the importance of the self-assemblies. The overall consumption of the ester was also significantly higher at the acidic pH.

Feedback from pH variation allows regelation (two cycles)

It was noted that the pH of the system had a remarkable impact on the lifetimes of gels, the extent of self-assembly, and the subsequent negative feedback from hydrolysis (Fig. 2e–g). We envisaged that if the system can itself register an autonomous gradual pH drop that is synchronized with the time delay in catalysis, it might be possible to realize additional cycles of (dis)assembly; an important observation in the literature thus far (Figs. 1c and 3a). The slowly forming waste (**B**) generated via hydrolytic cleavage of **BC** can be the proton source to independently decrease the environmental pH that can consequently facilitate the regeneration of **A'BC** utilizing the remaining ester in the medium to restart the cycle (Fig. 3a). Hence, unbuffered medium (Milli Q water) was used to generate the pH gradient within the medium. The mixture of **A'** and **BC** (50: 50 mM, **Sol1**) in 60% v/v DMSO/water showed an initial pH of 7.35 due to the presence of **A'**. To monitor whether the in-situ generation of **B** was able to increase the acidity of the system, the pH was measured with time. Indeed, the pH of the system gradually declined from 7.35 to 6.1 in a span of ca. 48 h (Fig. 3d). The visible light scattering measurement of the unbuffered system showed an increase in turbidity till 2 h that was followed by an

https://doi.org/10.1038/s41467-024-54197-y

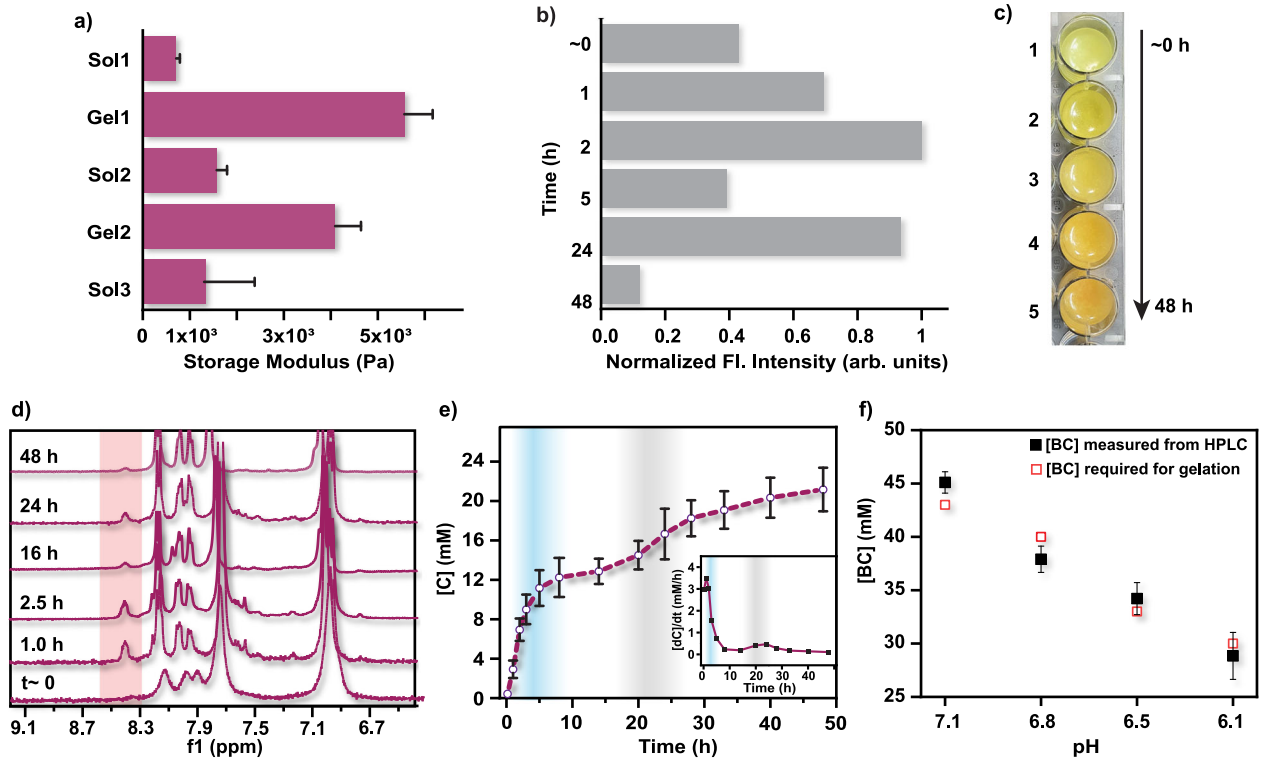

Fig. 4 | Temporal generation of self-assembly and its catalytic activity. a Time-dependent rheology showing the autonomous change in mechanical strength in the unbuffered system. **b** Time-dependent change in fluorescence intensity in the unbuffered system using DPH (λ_{ex} = 350 nm). **c** pH-dependent color change of Methyl Red indicator in unbuffered system. **d** Time-dependent ^{1}H NMR in unbuffered medium. **e** Time-dependent HPLC showing the generation of **C** in unbuffered system. Inset shows the first derivative plot for better visualization of the increased hydrolytic rate (blue and gray bands). Error bars represent standard deviations of triplicate experiments. **f** Concentration of **BC** required for gelation at different pHs (red square) and concentration of **BC** in unbuffered system measured from HPLC at different pHs (black square).

expected decline. Remarkably, a distinct increase of turbidity was observed after 15 h, which again peaked at 24 h followed by a substantial decline in intensity (Fig. 3e). This observation suggested that the phenomenon of the creation of catalytic microenvironment was registered twice as a function of time with a single batch of reactant addition (closed system). Further, visual observation reinforced the periodic change of (dis)assembly in unbuffered condition (Fig. 3b). Starting from the initial sol state (**Sol1**), a self-supporting gel (**Gel1**) was accessed at ~1.5–2 h which converted into sol (**Sol2**) approximately within 5 h (Fig. 3b). The regelation was observed at ca. 23–24 h (**Gel2**, Fig. 3b). This was followed by the formation of viscous solution (**Sol3**) in 60% of the samples while the rest 40% remained as weak gel after ca. 48 h (done in 10 different sets of vials under identical experimental conditions, Fig. 3b).

Moreover, two cycles of (dis)assembly were also suggested from time-dependent TEM investigations. Distinct network-like morphologies were seen to be accessed at ca. 2 h and 24 h, respectively, while in other time periods, a significantly lesser extent of networks was observed (Fig. 3c). Time-resolved rheology could also register the temporal generation and regeneration of higher mechanical strength of the **Gel1** and **Gel2** in the 1st and 2nd cycle, respectively. The higher storage modulus (G′) value of the **Gel1** (G′ = 5567 Pa) and **Gel2** (G′ = 4092 Pa) states compared to **Sol1** (G′ = 709 Pa), **Sol2** (G′ = 1572 Pa) and **Sol3** (G′ = 1310 Pa) underpinned the autonomous development of self-assembled structures at **Gel1** and **Gel2** states that resulted in gelation (Fig. 4a). To gain more details about the self-assembly process, time-dependent fluorescence spectroscopy was performed. DPH was used as a dye, a well-known fluorescent reporter that shows augmented intensity when bound to hydrophobic microenvironment[56]. Expectedly, in the 1st cycle (**Sol1**-**Gel1**-**Sol2**), a gradual increase in fluorescence intensity was observed, which peaked at **Gel1** state around 2 h, then started to decrease at 3 h (Fig. 4b). Around 24 h re-intensification of fluorescence intensity was observed followed by a decrease with ageing (Fig. 4b). The real-time pH change in the macroscopic gel was monitored by using Methyl Red indicator that was added to the system from *t*-0 h. The temporal change in color of the medium from yellow to orange demonstrated the autonomous drop of the pH within the system (Fig. 4c).

Further, time-dependent NMR was performed with the unbuffered system. As expected, the generation of imine proton peak was observed at δ 8.41 ppm, which gradually intensified at ca. 1 h (**Gel1**) followed by the decline in peak intensity (Fig. 4d). The peak registered a resurgence in intensity at around 20-24 h (**Gel2**, Fig. 4d). Subsequently, the imine proton peak started to diminish after 24 h and plateaued around 48 h. This result supported that, indeed, the waste **B** helped to induce positive feedback to regenerate the imine within the unbuffered system, and consequently, re-assembly was observed. Also, we did not observe any imine peak for the condensation of **A′** and waste **B**, which suggested that the self-assembly potential of **A′BC** helped in its own formation.

Extensive time-dependent HPLC was performed to monitor the release of **C** with respect to time and the hydrolytic activity. As hypothesized, the positive feedback from pH, which resulted in the re-formation of imine and subsequent regelation, was expected to play a critical role in reviving the hydrolytic capability. Indeed, after the plateauing of rates (first cycle, 9–15 h), an increase in the production rate of **C** could be detected again, at the similar timeline where regelation and re-intensification of imine were observed (Fig. 4e, gray band, 19–24 h).

After confirming the transient oscillation of the assembled state, the concentration distribution of the substrate as well as the products

https://doi.org/10.1038/s41467-024-54197-y

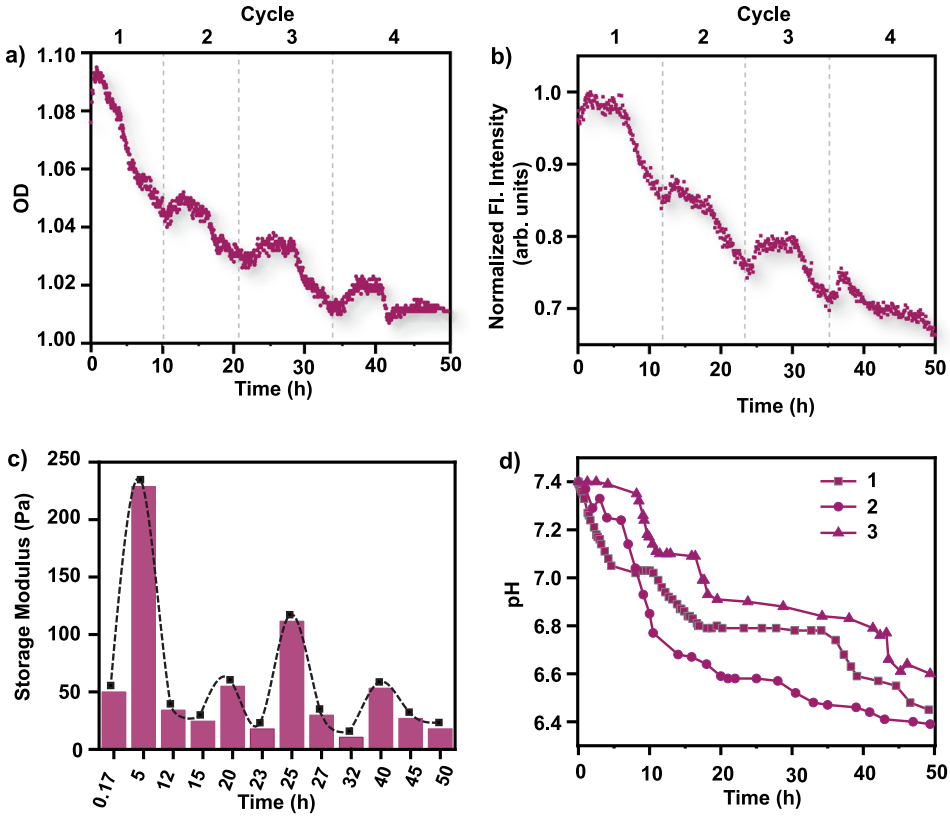

Fig. 5 | Multiple cycles of (dis)assembly in a closed system containing A* and BC in unbuffered condition. a Change in optical density with time (see Supplementary Fig. 11 for additional data sets). **b** Time-dependent change in fluorescence intensity of DPH (λ_{ex} = 350 nm, see Supplementary Fig. 12 for additional data sets). **c** Time-dependent change in storage modulus. Dotted line to guide the eye. **d** pH change as a function of time, the given data are taken from three independent experiments to confirm the monotonic pH drop.

that were presented and produced within the medium were quantified from HPLC (Fig. 4e). Initially, at high pH the higher concentration of the **BC** drove the gelation thus overcoming the low imine conversion rate. Whereas in the case of **Gel2**, the low pH of the system helps in the rapid imine formation, thus the gel was formed even at low concentrations of **BC**. With further decrease in pH no gel was formed because of insufficient concentration of ester at pH 6.1. In order to gain more insight into the (re)gelation process, control experiment was done to probe ex-situ the critical concentration of **BC** (in presence of [**A'**] = 50 mM) required for gelation at different pH values. Interestingly, the critical concentrations at pH 7.1 and pH 6.5 were lower than the concentrations of **BC** calculated from HPLC for the in-situ system at pH 7.1 (ca. 1.5 h) and pH 6.5 (ca. 22.4 h, Fig. 4f). However, the ex situ critical concentrations of **BC** required for gelation at pH 6.8 and pH 6.1 were higher than the concentrations found (from HPLC) in the in-situ system at pH 6.8 (ca. 9.4 h) and pH 6.1 (ca. 48 h, Fig. 4f). In combination, these results suggested that the concentrations of **BC** as a function of pH and time play a critical role in (dis)assembly process. The fact that the consumption of a thermodynamically activated ester drives the multiple cycles of (dis)assembly of the building block as a function of time suggests the non-equilibrium nature of the system[2,14].

The (dis)assembly observed in the system containing **A'** and **BC** for only two cycles can be attributed to the insufficient remaining amount of **BC** for re-assembly, considering the higher critical aggregation concentration of the system. Hence, we speculated that if additional hydrogen bonding capabilities could be installed in the system, the CAC would be lowered, providing the opportunity to (dis)assemble for multiple cycles. In this regard, a new building block **A*** (a dipeptide of histidine and β-alanine with an amide for additional hydrogen bonding) as a replacement of **A'** was used along with **BC** at 1:1 (25:25 mM, 60% DMSO/water, pH 7.4), and the system was probed by various techniques based on ensemble measurements. Indeed, the system displayed a periodic variation in optical density which suggested the transient oscillation (Fig. 5a, Supplementary Fig. 11, 4 out of 8 individual experiments showed multiple cycles). The fluorescence experiment performed in the presence of DPH revealed a similar pattern of autonomous increase and decrease in intensity for multiple cycles, suggesting the temporal changes in the hydrophobic domains (Fig. 5b, Supplementary Fig. 12, 4 out of 8 individual experiments showed four cycles). The mechanical strength of the system also showed multiple cycles of increase and decrease in storage modulus suggesting the process of the (de)generation of the assemblies although visually we did not observe gelation (Fig. 5c). HRMS data of the phase (turbid solution) that possessed high storage modulus solution (ca. ~5 h) confirmed the presence of **A*BC** (Supplementary Fig. 13). Confocal laser scanning microscopy and TEM images suggested that **A*** based system accessed fibrous assemblies (Supplementary Fig. 14). Notably, the pH of the system showed an autonomous monotonic decrease in a stepwise fashion (Fig. 5d). Further, multiple experiments (UV, fluorescence, rheology and pH change) were performed from a single batch (one system) confirmed the periodic changes in (dis)assembly with coherence in the timeframe (Supplementary Fig. 15). Notably, in the context of monotonic stepwise pH change, seminal work by Field, Kőrös, and Noyes (known as the FKN model on BZ reaction, a chemical oscillator) suggest similar monotonic behavior in changes of some components such as malonic acid[57]. These observations highlighted that a simple variation of the building block led to multiple cycles of (dis)assembly, exploiting the nonlinearity of the time-coupled autonomous cyclic process of assembly-catalysis-pH drop-regeneration of building block-assembly (Fig. 1c).

https://doi.org/10.1038/s41467-024-54197-y

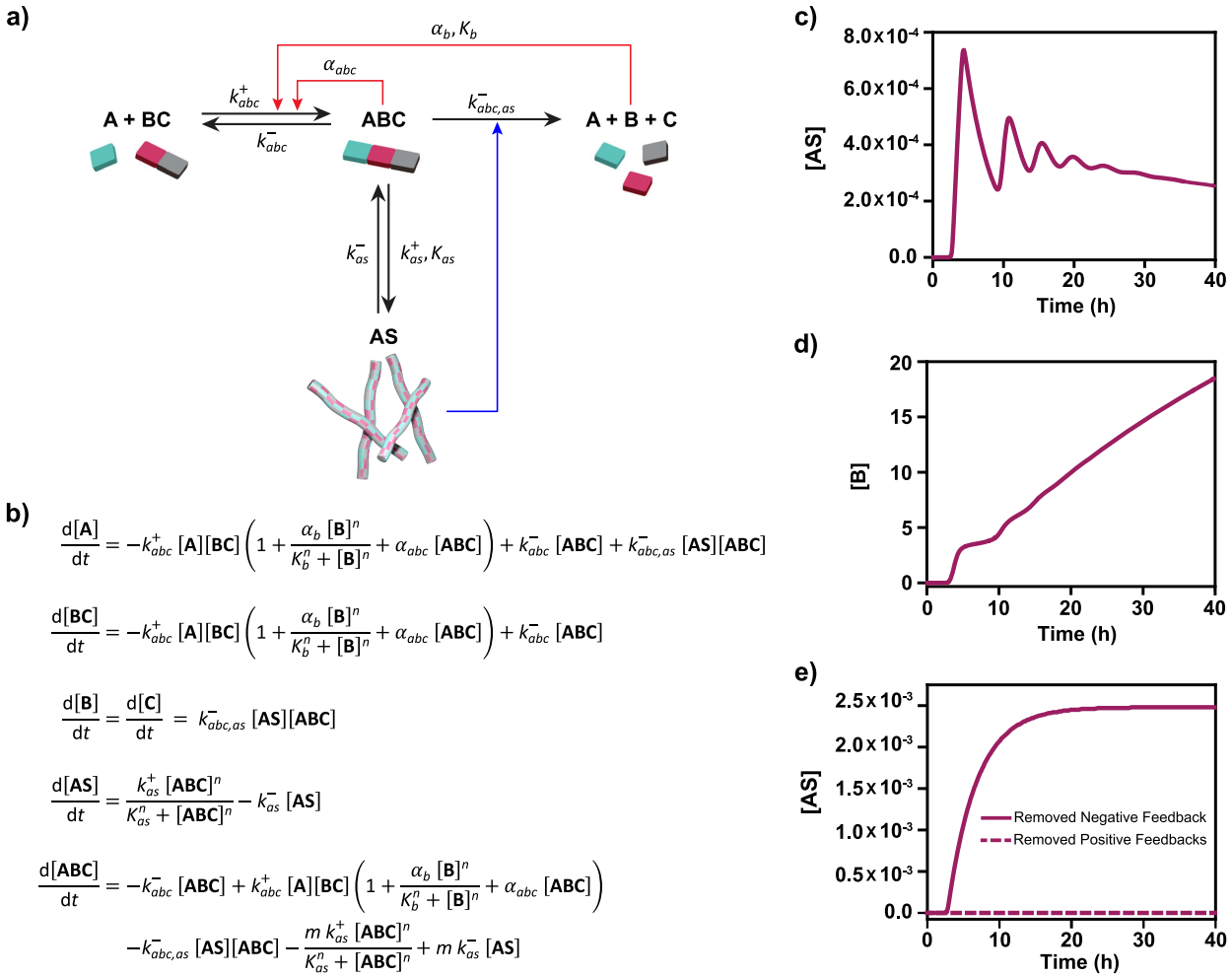

$$\frac{d[A]}{dt} = -k^{+}_{abc}[A][BC]\left(1+\frac{\alpha_b[B]^n}{K_b^n+[B]^n}+\alpha_{abc}[ABC]\right)+k^{-}_{abc}[ABC]+k^{-}_{abc,as}[AS][ABC]$$

$$\frac{d[BC]}{dt} = -k^{+}_{abc}[A][BC]\left(1+\frac{\alpha_b[B]^n}{K_b^n+[B]^n}+\alpha_{abc}[ABC]\right)+k^{-}_{abc}[ABC]$$

$$\frac{d[B]}{dt} = \frac{d[C]}{dt} = k^{-}_{abc,as}[AS][ABC]$$

$$\frac{d[AS]}{dt} = \frac{k^{+}_{as}[ABC]^n}{K_{as}^n+[ABC]^n}-k^{-}_{as}[AS]$$

$$\frac{d[ABC]}{dt} = -k^{-}_{abc}[ABC]+k^{+}_{abc}[A][BC]\left(1+\frac{\alpha_b[B]^n}{K_b^n+[B]^n}+\alpha_{abc}[ABC]\right)$$
$$-k^{-}_{abc,as}[AS][ABC]-\frac{m\,k^{+}_{as}[ABC]^n}{K_{as}^n+[ABC]^n}+m\,k^{-}_{as}[AS]$$

Fig. 6 | Mathematical modeling of periodic (dis)assembly. a Kinetic modeling scheme incorporating negative and positive feedback loops. **b** System of ordinary differential equations describing the kinetic model. **c** Representative simulation results for a single parameter set where multiple cycles of (dis)assembly were observed as transient peaks. **d** Concentration of **B** showed stepwise increase synchronized with assembly cycles. **e** Representative simulation results where the elimination of negative feedback and positive feedback completely abrogated the re-assembly.

Notably, this variation also suggested how the encoded chemical information in the structure of simple building blocks could dictate the number of cycles and periodic changes of (dis)assembly.

Kinetic model for the simulation of transient oscillation under non-equilibrium conditions

In order to establish a generalized qualitative scheme, a kinetic model was developed to theoretically predict whether periodic fluctuation is possible, to examine the contribution of the feedback loop, and to test whether a kinetic model is able to capture the non-linearity observed experimentally in the generation of the reaction products in this minimal chemical-based system. The model included the negative feedback originating from the assembly-mediated degradation of **ABC** (**A** = **A'** or **A***) and the positive feedback from pH-driven augmentation in the rate of **ABC** formation and the fact that the self-assembly process that drives the formation of **ABC** (as seen in Fig. 6a, for more details see section 3 in Supplementary Information). It was assumed that the formation of **ABC** promoted the rate of **ABC** generation linearly, while the pH-driven positive feedback via proton release (**B**) was modeled as a Hill function. In other words, it was assumed that a significant amplification of the **ABC** formation rate occurs only when the amount of **B** in the system reached a critical concentration, which aligned with experimental observations. The Hill function, being one of the simplest forms capable of describing such dynamics and critical concentration requirements, was hence used to model the **B**-mediated positive feedback loop. As seen experimentally, the degradation of **ABC** was formulated to occur only in the presence of the assembled state (**AS**), realizing a feedback loop. Hence, the kinetic model proposed here did not include **AS**-independent degradation of **BC**. Based on these assumptions, a mass balance for each component led to ordinary differential equations describing the change of each chemical species in the system (Fig. 6b). Theoretical analysis mathematically proved that this system is incapable of sustained oscillation irrespective of the specific values of the reaction rate constants and initial concentrations (see Supplementary Information, section 3.2). However, this does not preclude transient oscillation in the system when the system is far from the steady-state concentrations. Indeed, numerical simulations using estimated rate constants (see Supplementary Table 1) showed transient oscillation of the assembled state (**AS**, Fig. 6c). [**AS**], though represented as a concentration, defines the extent of assembly and not a concentration. The model could further simulate the stepwise increase in concentration of **B**, which corroborates the experimentally observed formation of **B** as a function of time (Figs. 5d and 6d). The concentrations predicted by the numerical simulations of the proposed model using the estimated rate constants are consistent with the experimentally observed kinetics.

For numerical simulations, the Hill coefficient (n) was set to 5, and the stoichiometric coefficient (m) was assumed to be 100. Although

[**AS**] represents the concentration of polymers of size *m* that are composed of **ABC** subunits, we consider it as a proxy for the extent of assembly in the system and not a concentration. The purpose of this modeling exercise was not to develop a mathematical model that precisely replicates experimental results but rather to demonstrate that a closed reaction network constructed using known chemistry can exhibit transient oscillations. Consequently, we focus on the qualitative behavior of the assembled state instead of making quantitative predictions. In line with this approach, the phenomenological model presented here combines elementary reactions occurring in the system into single expressions or rate constants.

To investigate the role of feedback loops in sustaining periodic (dis)assembly, the proposed model was simulated using the selected parameter sets after systematically eliminating negative feedback and positive feedbacks one at a time (Fig. S16, see Supplementary Information for details, section 3.7). Initially, the negative feedback was eliminated, which resulted in continual generation of assembled state with complete abrogation of (dis)assembly cycles (Fig. 6e, solid line). Then, the two positive feedbacks (i.e., pH-driven augmentation in the rate of **ABC** formation and assembly promoted **ABC** generation) were simultaneously removed (Fig. 6e, dotted line). The removal of the two positive feedbacks completely halted the assembly, highlighting their essential role in transient oscillation (see section 3.7 in Supplementary Information). The results underpin that the precise integration of the negative and positive feedback loops within the system played a critical role in maintaining the (dis)assembly cycle.

Moreover, the robustness of the model was validated by varying the initial conditions of the substrates (**A** and **BC**) and the rate constants up to two-fold (Supplementary Fig. 17, see section 3.8 in Supplementary Information for details). Variations in the Hill coefficient did not influence the qualitative outcomes of this study, as the model robustly generated transient oscillations regardless of the specific value of *n*. Similarly, results were found to be independent of the value of the stoichiometric constant *m*. This kinetic model illustrated how rudimentary chemical interactions, coupled with feedback loop, could be applied to analyze the onset of transient oscillation in a general system.

Discussion

Modern-day organisms rely on elaborate and complex interconnected networks of non-equilibrium metabolic pathways with evolved enzymes for the construction (anabolism) and degradation (catabolism) of molecules for the maintenance of homeostasis. Living systems engage both non-covalent assembly and covalent linkages to achieve such complex behaviors. This work demonstrates a simple chemical network that uses only two components, a single amino acid/dipeptide and a thermodynamically activated small molecular ester, to demonstrate complex dynamic behavior such as the capability to show feedback-driven transient oscillation where the (dis)assembly behavior demonstrated periodic changes with a single batch addition of reactants. The system exploits non-covalent assembly, which results in acceleration of catalysis and generation of non-linear pH gradient, which leads to regeneration of a dynamic covalent bond, to install a feedback loop in the closed system. Although the system could not exhibit true oscillatory behavior, yet this can serve as an example of a minimal synthetic network that can demonstrate periodic behaviors in a closed system, especially in the absence of advanced biocatalytic systems.

Methods

Materials

L-histidine (99 %), 4-nitrophenol (98 %), and benzoic acid (99 %) were purchased from SRL Chemicals, India. 4-formylbenzoic acid (98 %), HEPES (N-(2-Hydroxyethyl) piperazine-N′-(2-ethanesulfonic acid) (98 %), MES (2-(N-morpholino) ethanesulfonic acid) (98 %), PTSA monohydrate (p-Toluenesulfonic acid, 98 %) and trifluoro acidic acid (TFA, 99 %) were purchased from TCI, India. Carnosine (98 %) was purchased from BLD Pharm. Dimethyl sulfoxide (DMSO), HPLC water, acetonitrile (ACN), and all other solvents were purchased from Sigma Aldrich Merck.

NMR studies

All ^{1}H NMR spectra of the synthesized compounds were recorded in JEOL (400 MHz) at 25 °C in respective solvents. To monitor the time-dependent ^{1}H NMR, we prepared the sample within the vial and then transferred the mixture into an NMR tube, followed by the recordation of the scan at different time intervals. The temperature was maintained at 25 ± 1 °C throughout the experiment.

Turbidity measurement

The turbidity was monitored using an Agilent Cary 3500 UV-Visible spectrophotometer. All Histidine (**A'**) containing samples were prepared following the same procedure as mentioned before and were transferred to demountable cells of path length of 0.1 mm to perform the experiment.

The time-dependent absorbances of the different samples were monitored at 700 nm wavelength.

Optical density measurement

A* was dissolved in Milli Q water (~pH 7.4, pH was adjusted to 7.4 by the addition of 1 N HCl) by heating at around 80 °C followed by the addition of DMSO solution of **BC** to drive the assembly and the final concentration of **A*:BC** was maintained at 25:25 mM. Then the samples were transferred to a 96-well plate and monitored in BioTek Synergy H1 microplate reader.

The time-dependent OD of the different samples was monitored at 700 nm wavelength.

Transmission electron microscopy

To prepare the samples, each system was diluted by 60% DMSO/H_2O, drop cast on the TEM grid, and left for 120 s to allow the adsorption on the grid. The excess solution was then wicked off with a piece of filter paper. The contrast was achieved by staining with 1 wt % uranyl acetate solution, and after 60 s, the excess staining agent was removed by using filter paper. The samples were further dried for 8 h in vacuo at 4 °C before imaging and kept overnight under in vacuo. Images were recorded in JEOL JEM-2100F microscope.

Scanning electron microscopy

SEM measurements were recorded on a Carl Zeiss SUPRA 55VP instrument. The samples were prepared following a similar protocol to that for TEM except the addition of the staining agent, and they were cast on the silicon wafer.

Rheology measurement

The rheological experiments were carried out in an Anton Paar rheometer (MCR-102) equipped with parallel plates (PP08/PE). To realize the mechanical strength of all the systems, a frequency sweep experiment was done using the fixed strain at 0.1%. To obtain the viscoelastic region of the gel, an initial strain sweep experiment was performed using the different ranges of strain from 0.01 to 100% at a constant oscillatory frequency of 1 Hz. The mechanical property was monitored at a constant strain of 0.1% and constant frequency (1 Hz) at 25 °C at different time intervals.

High-performance liquid chromatography

Analytical HPLC was performed with Waters HPLC system equipped with 1525 binary pump and 2998 photodiode array detector by using XBridge C18 5 μm 4.6 × 250 mm analytical HPLC column. The flow rate was maintained at 1 mL/min with a gradient elution method by using 0.1% TFA ACN and 0.1% TFA water as the mobile phase. Samples were diluted with 50% ACN (0.1% TFA)/water (0.1% TFA) before each

injection. To monitor the kinetics of the formation of **B** and the consumption of **BC**, chromatograms were extracted at 318 nm and 265 nm, respectively. Mesitylene was used as an internal standard.

pH measurement

The time-dependent pH of the systems containing **A'** + **BC** and **A*** + **BC** was monitored by using Horiba Laqua twin pH 22 and Eutech Instruments pH 700.

Fluorescence spectroscopy study

Fluorescence spectra for **A'** + **BC** system were recorded by using an Agilent Cary Eclipse spectrofluorometer using a slit-width of 10 nm. 1,6-diphenyl-1,3,5-hexatriene (DPH) was added at the initial time of sample preparation and placed in a cell of 10 mm path length for time-dependent fluorescence measurement. The final concentration of the DPH was maintained at 10 μM. The samples were excited at 350 nm.

Fluorescence spectra for the **A*** + **BC** system were recorded by using BioTek Synergy H1 microplate reader using gain value 50. DPH was added at the initial time of sample preparation and placed in the black 96-well plate for time-dependent fluorescence measurement. The final concentration of the DPH was maintained at 20 μM. The samples were excited at 350 nm.

Confocal microscopy

The images were collected in Olympus Laser Scanning Confocal System Model FV3000 (part of the Atomic Force Microscope with Rheological Measurement and Confocal Imaging Unit Facility, supported by Swarnajayanti (SB/SJF/2020-21/08)).

The system containing **A*** + **BC** was diluted with 60% DMSO/Water, and Nile Red was added to the system, followed by incubation for 10 min. After that, the solution was drop casted over the glass slide and confocal images were recorded using the same instrument.

Experiments conducted with samples taken from a single vial (one system containing A* + BC)

A large volume of solution (5 ml) was initially prepared to conduct different experiments (UV, fluorescence, rheology, and pH) with the samples taken from a single system. In each experiment, a required amount of the aliquot was taken from the solution containing **A*** + **BC**, and data points were subsequently recorded. However, it is important to note here one out of four such systems showed coherence in the experimental data (UV, fluorescence, rheology and pH).

Data availability

The authors declare that all data supporting this work are contained in graphics displayed in the main text or in the Supplementary Information. Data used to generate these graphics are available from the authors upon request. Source data are provided with this paper.

References

1. Grzybowski, B. A. & Huck, W. T. S. The nanotechnology of life-inspired systems. *Nat. Nanotechnol.* **11**, 585–592 (2016).
2. Ragazzon, G. & Prins, L. J. Energy consumption in chemical fuel-driven self-assembly. *Nat. Nanotechnol.* **13**, 882–889 (2018).
3. He, X. et al. Synthetic homeostatic materials with chemo-mechano-chemical self-regulation. *Nature* **487**, 214–218 (2012).
4. Bal, S., Ghosh, C., Ghosh, T., Vijayaraghavan, R. K. & Das, D. Non-equilibrium polymerization of cross-β amyloid peptides for temporal control of electronic properties. *Angew. Chem. Int. Ed.* **59**, 13506–13510 (2020).
5. Ashkenasy, G., Hermans, T. M., Otto, S. & Taylor, A. F. Systems chemistry. *Chem. Soc. Rev.* **46**, 2543–2554 (2017).
6. Das, K., Gabrielli, L. & Prins, L. J. Chemically fueled self-assembly in biology and chemistry. *Angew. Chem. Int. Ed.* **60**, 20120–20143 (2021).
7. Boekhoven, J., Hendriksen, W. E., Koper, G. J. M., Eelkema, R. & van Esch, J. H. Transient assembly of active materials fueled by a chemical reaction. *Science* **349**, 1075–1079 (2015).
8. Wang, J., Abbas, M., Wang, J. & Spruijt, E. Selective amide bond formation in redox-active coacervate protocells. *Nat. Commun.* **14**, 8492 (2023).
9. Debnath, S., Roy, S. & Ulijn, R. V. Peptide nanofibers with dynamic instability through nonequilibrium biocatalytic assembly. *J. Am. Chem. Soc.* **135**, 16789–16792 (2013).
10. Ottelé, J., Hussain, A. S., Mayer, C. & Otto, S. Chance emergence of catalytic activity and promiscuity in a self-replicator. *Nat. Catal.* **3**, 547–553 (2020).
11. Kroiss, D., Ashkenasy, G., Braunschweig, A. B., Tuttle, T. & Ulijn, R. V. Catalyst: can systems chemistry unravel the mysteries of the chemical origins of life? *Chem* **5**, 1917–1923 (2019).
12. Miljanic, O. S. Small-molecule systems chemistry. *Chem* **2**, 502–524 (2017).
13. Chen, C. et al. Design of multi-phase dynamic chemical networks. *Nat. Chem.* **9**, 799–804 (2017).
14. Astumian, R. D. Kinetic asymmetry allows macromolecular catalysts to drive an information ratchet. *Nat. Commun.* **10**, 3837 (2019).
15. Gentile, S., Del Grosso, E., Prins, L. J. & Ricci, F. Autonomous and programmable reorganization of DNA-based polymers using redox chemistry. *Chem. Eur. J.* **29**, e202300394 (2023).
16. Leira-Iglesias, J., Tassoni, A., Adachi, T., Stich, M. & Hermans, T. M. Oscillations, travelling fronts and patterns in a supramolecular system. *Nat. Nanotechnol.* **13**, 1021–1027 (2018).
17. Liu, K. et al. Light-driven eco-evolutionary dynamics in a synthetic replicator system. *Nat. Chem.* **16**, 79–88 (2024).
18. De, S. & Klajn, R. Dissipative self-assembly driven by the consumption of chemical fuels. *Adv. Mater.* **30**, 1706750 (2018).
19. Westerhoff, H. V., Tsong, T. Y., Chock, P. B., Chen, Y.-D. & Astumian, R. D. How enzymes can capture and transmit free energy from an oscillating electric field. *Proc. Natl Acad. Sci. USA* **83**, 4734–4738 (1986).
20. Hermans, T. M. & Singh, N. Chemically fueled autonomous Sol→Gel→Sol→Gel→Sol transitions. *Angew. Chem. Int. Ed.* **62**, e202301529 (2023).
21. Di. Noja, S., Garrido, M., Gualandi, L. & Ragazzon, G. Control over dethreading kinetics allows evaluating the entropy stored in an interlocked molecular machine out-of-equilibrium. *Chem. Eur. J.* **29**, e202300295 (2023).
22. Weißenfels, M., Gemen, J. & Klajn, R. Dissipative self-assembly: fueling with chemicals versus light. *Chem* **7**, 23–37 (2021).
23. Semenov, S. N. et al. Autocatalytic, bistable, oscillatory networks of biologically relevant organic reactions. *Nature* **537**, 656–660 (2016).
24. Kleeb, A. C. et al. Metabolic engineering of a genetic selection system with tunable stringency. *Proc. Natl Acad. Sci. USA* **104**, 13907–13912 (2007).
25. Ferrell, J. E. Jr, Tsai, T. Y.-C. & Yang, Q. Modeling the cell cycle: why do certain circuits oscillate? *Cell* **144**, 874–885 (2011).
26. Hazen, R. M., Griffin, P. L., Carothers, J. M. & Szostak, J. W. Functional information and the emergence of biocomplexity. *Proc. Natl Acad. Sci. USA* **104**, 8574–8581 (2007).
27. Wagner, N., Hochberg, D., Peacock-Lopez, E., Maity, I. & Ashkenasy, G. Open prebiotic environments drive emergent phenomena and complex behavior. *Life* **9**, 45 (2019).
28. Dai, K. et al. Spontaneous and selective peptide elongation in water driven by aminoacyl phosphate esters and phase changes. *J. Am. Chem. Soc.* **145**, 26086–26094 (2023).
29. Semenov, S. N. et al. Rational design of functional and tunable oscillating enzymatic networks. *Nat. Chem.* **7**, 160–165 (2015).

30. Howlett, M. G., Engwerda, A. H. J., Scanes, R. J. H. & Fletcher, S. P. An autonomously oscillating supramolecular self-replicator. *Nat. Chem.* **14**, 805–810 (2022).
31. Rosier, B. J. H. M. & de Greef, T. F. A. Synthetic biology: how to make an oscillator. *eLife* **4**, e12260 (2015).
32. Klemm, B., Lewis, R. W., Piergentili, I. & Eelkema, R. Temporally programmed polymer–solvent interactions using a chemical reaction network. *Nat. Commun.* **13**, 6242 (2022).
33. Grzelczak, M., Liz-Marzán, L. M. & Klajn, R. Stimuli-responsive self-assembly of nanoparticles. *Chem. Soc. Rev.* **48**, 1342–1361 (2019).
34. Deng, J. & Walther, A. Pathway complexity in fuel-driven DNA nanostructures with autonomous reconfiguration of multiple dynamic steady states. *J. Am. Chem. Soc.* **142**, 685–689 (2020).
35. Colomer, I., Morrow, S. M. & Fletcher, S. P. A transient self-assembling self-replicator. *Nat. Commun.* **9**, 2239 (2018).
36. Mishra, A. et al. Biomimetic temporal self-assembly via fuel-driven controlled supramolecular polymerization. *Nat. Commun.* **9**, 1295 (2018).
37. Dev, D. et al. A Peptide-Based Oscillator. *J. Am. Chem. Soc.* **145**, 26279–26286 (2023).
38. Pramanik, S. & Aprahamian, I. Hydrazone switch-based negative feedback loop. *J. Am. Chem. Soc.* **138**, 15142–15145 (2016).
39. Freeman, M. Feedback control of intercellular signalling in development. *Nature* **408**, 313–319 (2000).
40. Heinen, L., Heuser, T., Steinschulte, A. & Walther, A. Antagonistic enzymes in a biocatalytic pH feedback system program autonomous DNA hydrogel life cycles. *Nano Lett.* **17**, 4989–4995 (2017).
41. Gyorgyi, L., Turányi, T. & Field, R. J. Mechanistic details of the oscillatory Belousov-Zhabotinskii reaction. *J. Phys. Chem.* **94**, 7162–7170 (1990).
42. Ragazzon, G. et al. Autonomous non-equilibrium self-assembly and molecular movements powered by electrical energy. *Angew. Chem. Int. Ed.* **62**, e202214265 (2023).
43. Novák, B. & Tyson, J. Design principles of biochemical oscillators. *Nat. Rev. Mol. Cell Biol.* **9**, 981–991 (2008).
44. Tsai, T. Y.-C. et al. tunable biological oscillations from interlinked positive and negative feedback loops. *Science* **321**, 126–129 (2008).
45. Orbán, M., Kurin-Csörgei, K. & Epstein, I. R. pH-regulated chemical oscillators. *Acc. Chem. Res.* **48**, 593–601 (2015).
46. ter Harmsel, M. et al. A catalytically active oscillator made from small organic molecules. *Nature* **621**, 87–93 (2023).
47. Li, X. et al. Selenium catalysis enables negative feedback organic oscillators. *Nat. Commun.* **15**, 3316 (2024).
48. Johnson, B. R., Scott, S. K. & Thompson, B. W. Modelling complex transient oscillations for the BZ reaction in a batch reactor. *Chaos* **7**, 350–358 (1997).
49. Omosun, T. O. et al. Catalytic diversity in self-propagating peptide assemblies. *Nat. Chem.* **9**, 805–809 (2017).
50. Sheehan, F. et al. Peptide-based supramolecular systems chemistry. *Chem. Rev.* **121**, 13869–13914 (2021).
51. Rieu, T., Osypenko, A. & Lehn, J. M. Triple adaptation of constitutional dynamic networks of imines in response to micellar agents: internal uptake–interfacial localization–shape transition. *J. Am. Chem. Soc.* **146**, 9096–9111 (2024).
52. Panja, S. & Adams, D. J. Stimuli responsive dynamic transformations in supramolecular gels. *Chem. Soc. Rev.* **50**, 5165–5200 (2021).
53. Chen, Y. et al. Self-assembled peptide nano-superstructure towards enzyme mimicking hydrolysis. *Angew. Chem. Int. Ed.* **60**, 17164–17170 (2021).
54. Seoane, A., Brea, R. J., Fuertes, A., Podolsky, K. A. & Devaraj, N. K. Biomimetic generation and remodeling of phospholipid membranes by dynamic imine chemistry. *J. Am. Chem. Soc.* **140**, 8388–8391 (2018).
55. Clayden, J., Greeves, N. & Warren, S. G. Organic Chemistry. (Oxford University Press, Oxford, 2012).
56. Poojari, C. et al. Behavior of the DPH fluorescence probe in membranes perturbed by drugs. *Chem. Phys. Lipids* **223**, 104784 (2019).
57. Field, R. J., Koros, E. & Noyes, R. M. Oscillations in chemical systems. II. Thorough analysis of temporal oscillation in the bromate-cerium-malonic acid system. *J. Am. Chem. Soc.* **94**, 8649–8664 (1972).

Acknowledgements

D.D. is thankful to SB/SJF/2020-21/08 and MoE-STARS [STARS-2/2023-0752] Grant for financial assistance. A.R. acknowledges IISER Kolkata, and S.J. acknowledges UGC and PMRF. S.P. and S.B. acknowledge CSIR India for fellowships. C.G. and A.S. acknowledge funding from the Department of Biotechnology, Government of India, through grant BT/PR40128/BTIS/37/43/2022.

Author contributions

D.D. conceived and supervised the overall project. A.R. and S.J. contributed equally to the work. A.R., S.J., S.P., and S.B. conceived and performed all the experiments. A.S. and C.G. formulated the mathematical modeling and analysis strategy. A.S. carried out the mathematical analysis and numerical simulations. All authors participated in refining the reaction model structure and discussed simulation results. All authors co-wrote the paper, discussed the results, and commented on the manuscript.

Competing interests

The authors declare no competing interests.

Additional information

Supplementary information The online version contains supplementary material available at https://doi.org/10.1038/s41467-024-54197-y.

Correspondence and requests for materials should be addressed to Dibyendu Das.

Peer review information *Nature Communications* thanks Rein Ulijn for their contribution to the peer review of this work. A peer review file is available.